Int. J. Rock Mech. & Min. Sci. Vol. 34, No. 3-4, 1997
ISSN 0148-9062

To cite this paper:
Int. J. Rock Mech. & Min. Sci, **34:3-4**, Paper No. 00246

MICROSEISMICITY INDUCED BY A CONTROLLED, MINE COLLAPSE AT WHITE PINE, MICHIGAN

W. Scott Phillips, D. Craig Pearson, C.L. Edwards and Brian W. Stump

Earth and Environmental Sciences Division, Los Alamos National Laboratory
Los Alamos, NM 87545, USA

ABSTRACT

We recorded an explosively induced, 320 m deep, mine collapse and subsequent aftershocks at White Pine, Michigan, using an array of 12 seismic stations. The collapse resulted from the rubblization of a 3×10^4 m^2 panel of a room-and-pillar copper mine, performed to facilitate leaching operations. The explosions produced little seismic energy. However, the collapse generated strong tension-crack, free-fall and slap-down phases. Regional data indicate a magnitude (m_{bLg}) of 3.1, leading to estimates of displaced mass, 5.6×10^8 kg and thickness, 11 m. Peak acceleration was 300 cm/s^2 at ground zero and dropped to 20 cm/s^2 at 1.1 km.

Most of the locatable aftershocks (90%) occurred in the first 2 hours following collapse. At ground zero, the occurrence rate followed the modified Omori law: $Rate=560\cdot(time-0.01)^{-1.3}$, with time in hours. The largest aftershock generated a moment magnitude of 1.0. We obtained locations of 135 aftershocks. The aftershock zone was less than 100 m thick, situated on top of the collapsed panel. The shallowest aftershocks occurred at depths of 200 m, giving no indication of collapse-related deformation extending to the surface. Aftershocks concentrated along the only edge of the collapsed panel open to the room-and-pillar mine. If the seismically active area reflects the extent of the de-stressed zone used in modeling stress redistribution, the asymmetrical distribution with respect to the collapsed panel was consistent with lower-than-predicted stresses measured in the first row of intact pillars.

KEYWORDS

Geophysics, Seismic Monitoring, Mining, Acoustic Emission, Aftershocks, Case History, Collapse, Stress, Explosion, Comprehensive Test Ban Treaty.

INTRODUCTION

Our primary purpose in collecting seismic data during the 1995, controlled, mine collapse at White Pine, Michigan, was to learn to discriminate between mine collapse, nuclear test and other man-made and natural seismic events, which will be important under the new Comprehensive Test Ban Treaty (CTBT; United Nations, 1996). However, ground motions of the collapse and associated aftershocks yielded a wealth of information pertinent to mine engineering and environmental issues as well. In particular, the distribution and failure modes of the aftershocks should be related to the stress changes within and around the mine following collapse. Additionally, their distribution with depth may help evaluate any effect of the collapse on shallow

layers where the local, potable aquifer resides. In the following we will describe the collapse and aftershock data collected, analysis methods and results with emphasis on the aftershock location patterns.

SETTING

The White Pine Mine is located near Lake Superior on the Upper Peninsula of Michigan (Figure 1). The primary mineral mined is copper which was hydrothermally emplaced into low-grade, metamorphosed, sandstones and shales of pre-Cambrian age.

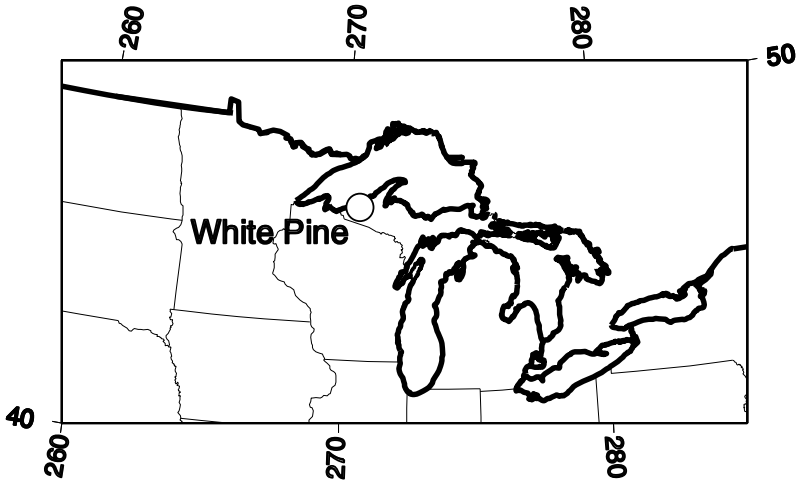

Figure 1: Location of the White Pine Mine, Upper Peninsula, Michigan.

The underground workings at the mine, shown in map view in Figure 2, are extensive, with rough dimensions of 8 km by 9 km. Historically, portions of the mine have collapsed "naturally." The naturally collapsed area in the north-central portion of the mine has collapsed slowly over a period of many years. The collapsed area to the south-west of the White Pine fault failed catastrophically January 14, 1988, producing locally felt ground motion (local magnitude 3.6) and extensive damage to underground mine structures.

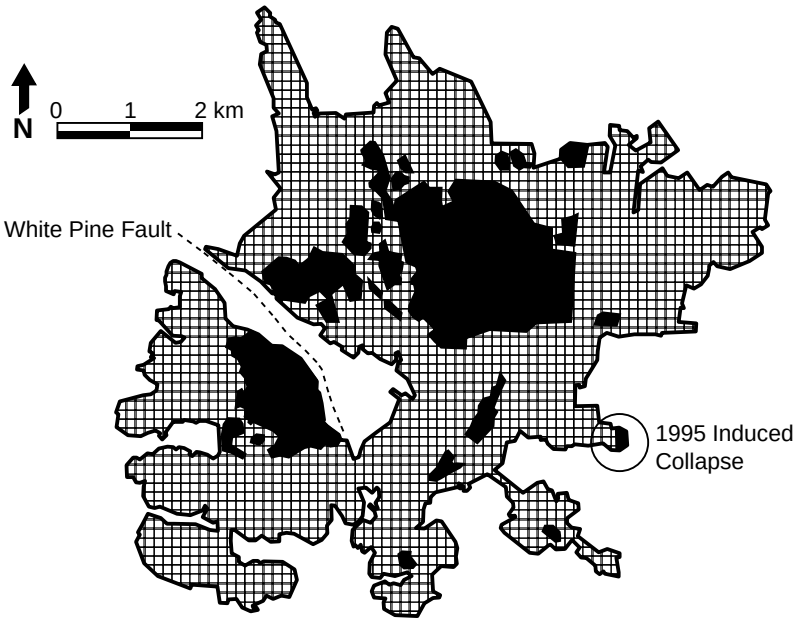

Figure 2: Plan view of underground workings at White Pine. The outer extent of room-and-pillar mining is outlined and failed pillar areas are indicated by black patches.

Recently discontinued operations at the mine relied on ore removal by room and pillar mining. A number of economic factors led to discontinuing the room and pillar operation and to investigating the effectiveness of pillar rubblization and in-situ leaching of the ore body remaining in the pillars. The controlled collapse documented here is the first of its type in the White Pine Mine.

A layer of glacial till, 10 to 20 m thick covers the surface at White Pine. The top of the water table is shallow, 1-2 m beneath the surface. Pre-Cambrian bedrock, consisting of Freda sandstone, Nonsuch shale and Copper Harbor conglomerate underlies the glacial till surface material. The mine follows the shale-conglomerate interface at a depth of 320 m in our study area. The depth to this interface varies laterally. These geological structures will be important to consider when calibrating the subsurface for microearthquake location purposes.

THE CONTROLLED MINE COLLAPSE

The pillar-removal operation was conducted on September 3, 1995 at 5:39 PM local time (246:21:39:38 UTM). Seventy-two (72) pillars with average dimensions of 6.1 m by 12.2 m were loaded with an average of 800 kg (1,807 lb.) of explosive per pillar for a total explosive source of 58,000 kg (130,068 lb.). A millisecond-delay firing pattern, 325 milliseconds in length, was used to minimize vibration effects at the surface and propagate the collapse toward the unmined faces. The area of the collapsed panel was roughly 3×10^4 m^2.

SEISMIC DATA ACQUISITION

Prior to the shot, Los Alamos personnel fielded a three-component, surface seismic network above the to-be-collapsed panel (Figure 3). Each station was instrumented with a six channel, Refraction Technology Model 72A-08 data logger which was continuously locked to GPS-broadcast timing signals. Three-component, 1 Hz, Mark Products Model L4-3C geophones were fielded at all but one station and a three-component, Terra Tech SSA-302 accelerometer was fielded at station 2. Sensors were deployed with horizontal components aligned to true north and east. Stations were programmed to record event-triggered data with the exception of station 13 (near surface ground zero) which recorded continuously. Stations 2 and 13 were digitized at 250 samples/s, other stations at 500 samples/s. Stations were located using handheld GPS receivers.

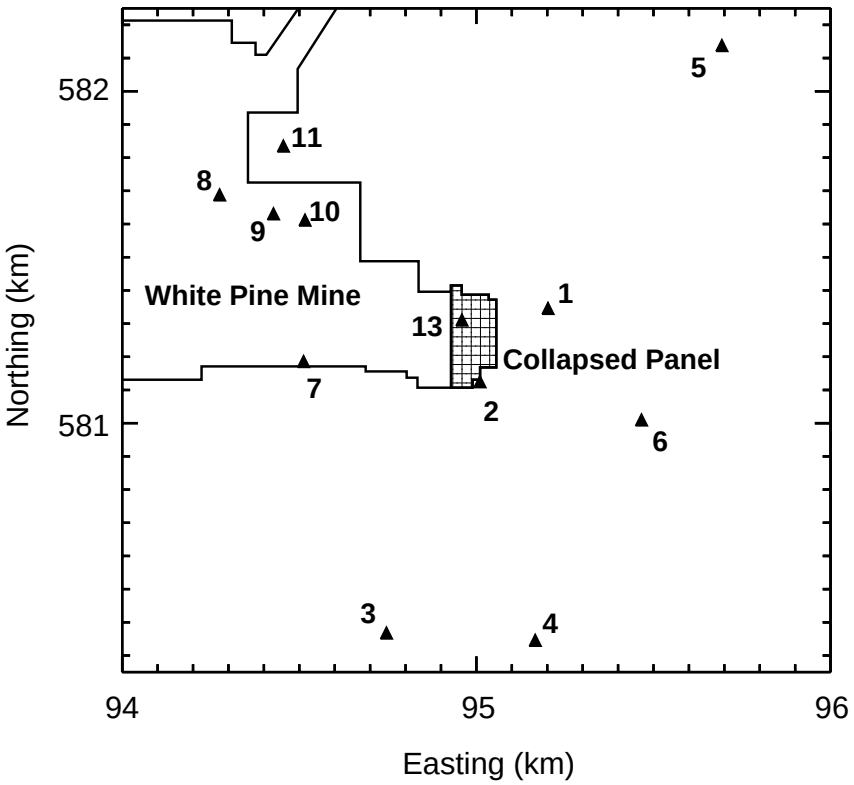

Figure 3: Map of three-component station locations (triangles). Mined areas and the collapsed panel are also indicated. Easting and northing are Michigan state coordinates.

THE EXPLOSIVELY INDUCED MINE COLLAPSE

Data

Figure 4 shows the ground motion at surface ground zero, where vertical motion was a factor of five larger than horizontal. The dominant motions shifted to the radial component with increasing distance from ground zero. At this amplification, the individual explosive sources in the pillars are not visible, but failure of the pillars and the mine back is indicated by the early high-frequency arrivals on the top trace. These failure signals ride on top of a long-period signal indicating an initially upward motion associated with the formation of a tensile crack and the release of material above the working level. This was followed by strong downward motion associated with the "slap down" of the released material.

Ground motion associated with pillar blasting was small, but can be seen if we amplify the signal immediately preceding the collapse, as shown by the bottom trace in Figure 4.

Peak acceleration reached 300 cm/s^2 at surface ground zero and fell to 20 cm/s^2 at station 5, 1.1 km distant. Peak velocities were 7 cm/s and 0.5 cm/s, respectively.

Regional seismograms were recovered from stations at ranges from 200 to 1000 km. Coda lengths at stations EYMN and TBO (150 s) indicated a body-wave magnitude (m_{bLg}) of 3.1 for the collapse event, using a scale developed for New England (Chaplin et al., 1980). We consider this magnitude an overestimate because Lg-coda attenuation is slightly higher in New England than in the north-central US (Singh and Herrmann, 1983).

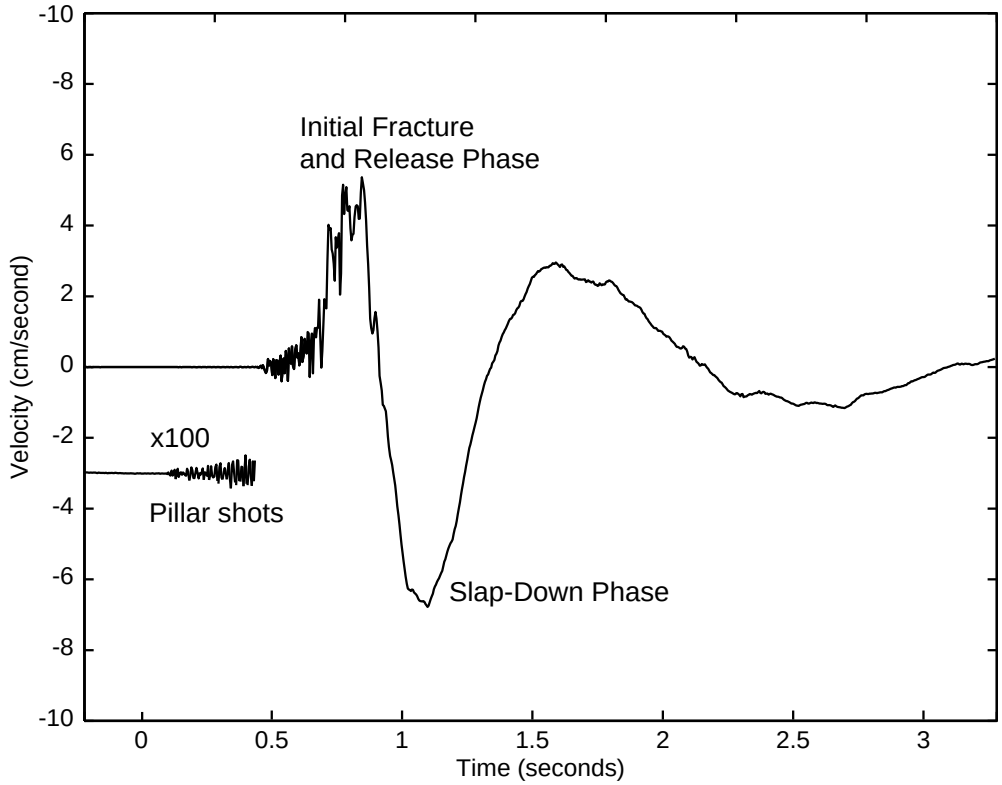

Figure 4: Vertical ground velocity at surface ground zero (station 13). The lower trace has been amplified a factor of 100 to show the pillar blasts. Time is measured from the origin time of the earliest pillar shot.

Discussion

The time between the release and slap-down phases of the collapse acceleration signal reflects the time of free-fall of the material above the mine workings. If the rooms are 2 m in height, free fall should take roughly 0.6 s. The free-fall time indicated by the data is 0.3 s or less (converting from velocity to acceleration, we take the time between inflection points on the first upward pulse of the seismogram in Figure 4), indicating a shorter

average fall of 0.5 m, presumably because of the rubblized pillars and bulking of fractured material from the mine back.

Following Taylor, 1994, we calculated the mass of falling material to be 5.6×10^8 kg. This was done using the body-wave magnitude of 3.1, and the free-fall distance of 0.5 m. Taking 2×10^4 m^2 as an estimate of the collapsed area (roughly 2/3 of the total area), a density of 2.5 gm/cm^3 and assuming a uniform thickness of the displaced material gave a thickness of 11 m. These must be considered rough estimates.

AFTERSHOCKS

Data

One hour of data from surface ground zero (station 13), starting with the mine collapse, are shown in Figure 5. Event rates approach 170 per minute at 6 minutes and fall off to under 4 per minute in two hours. We counted just over 4000 individual events in the 15 hours following collapse at the ground-zero station. The aftershock rate fit a modified Omori law (Utsu et al., 1995): $Rate=560\cdot(time-0.01)^{-1.3}$ (Figure 6). The fit was applied to data between 6 minutes and 15 hours after collapse. For times less than 6 minutes counting was incomplete. For time greater than 15 hours, a instrument malfunction increased noise levels and biased the counting.

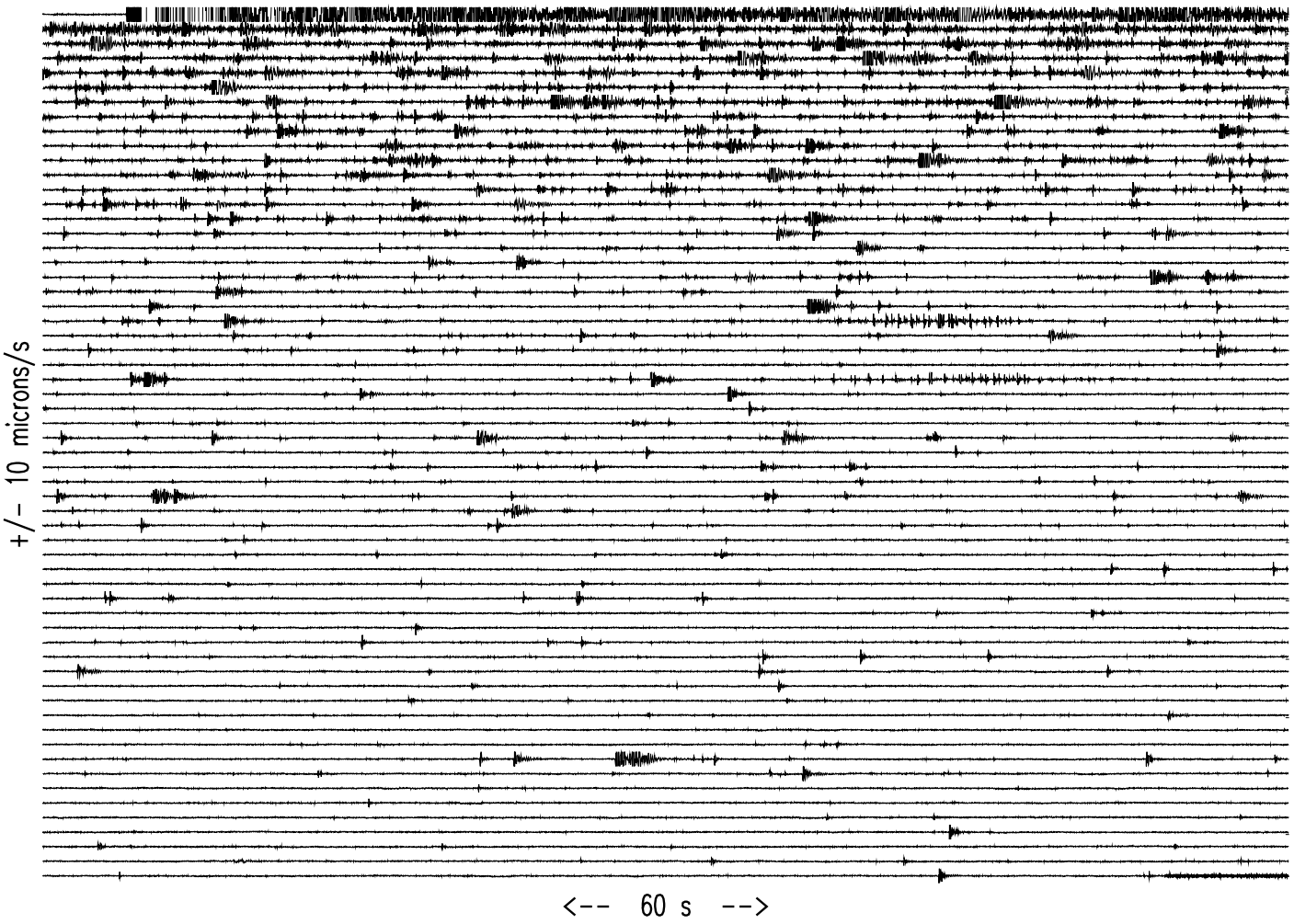

Figure 5: Station-13, vertical-component seismograms covering the first 1 hour following the collapse. The amplitude scale is fixed, causing larger events to be off scale. The strange signals at 22 and 26 minutes are scientists approaching ground zero to check equipment.

Over 90% of the locatable events (see next sections) occurred within 2 hours of the collapse. The remaining 10% occurred during isolated swarms of activity through the remaining 36 hours of network operation.

Ground motion from the largest aftershocks (moment magnitudes 1.0) was more than two orders of magnitude smaller than that of the collapse event. Seismograms displayed shear-slip and tensile-crack failure characteristics. A few of the largest events contained lower frequencies (10-20 Hz) and exhibited compressional motions at all stations, consistent with an explosion, or more likely, a tensile-crack source mechanism. However, these events typically contained significant S-wave arrivals. More commonly, aftershocks contained higher frequencies (up to 100 Hz) and exhibited high-amplitude S waves and both compressional and dilatational first motions, indicating a significant component of shear slip in the source mechanism (Figure 7). Compressions were most often observed at stations closest to ground zero (2 and 13) and dilatations at stations at a range of one depth-of-focus (320 m, 1 and 7). These observations are consistent with thrust-type shear-slip motion. These source-mechanism observations are preliminary and we will attempt to confirm them with moment-tensor studies at a later date.

Calibration and Location Methods

Calibration of the White Pine site consisted of creating layered, P- and S-wave velocity models of the subsurface as well as obtaining P- and S-wave station corrections. The station corrections accounted for lateral variations in the layer depths, which are known to be significant, and variations in the thickness of the glacial till layer at the surface. To calibrate, we used P- and S-wave arrival times from two, well-recorded microearthquakes, P-wave arrival times from the earliest pillar shot at innermost stations 1, 2, 7 and 13 (position fixed) and seismic reflection results (lines 7 and 8; Geosphere, 1995).

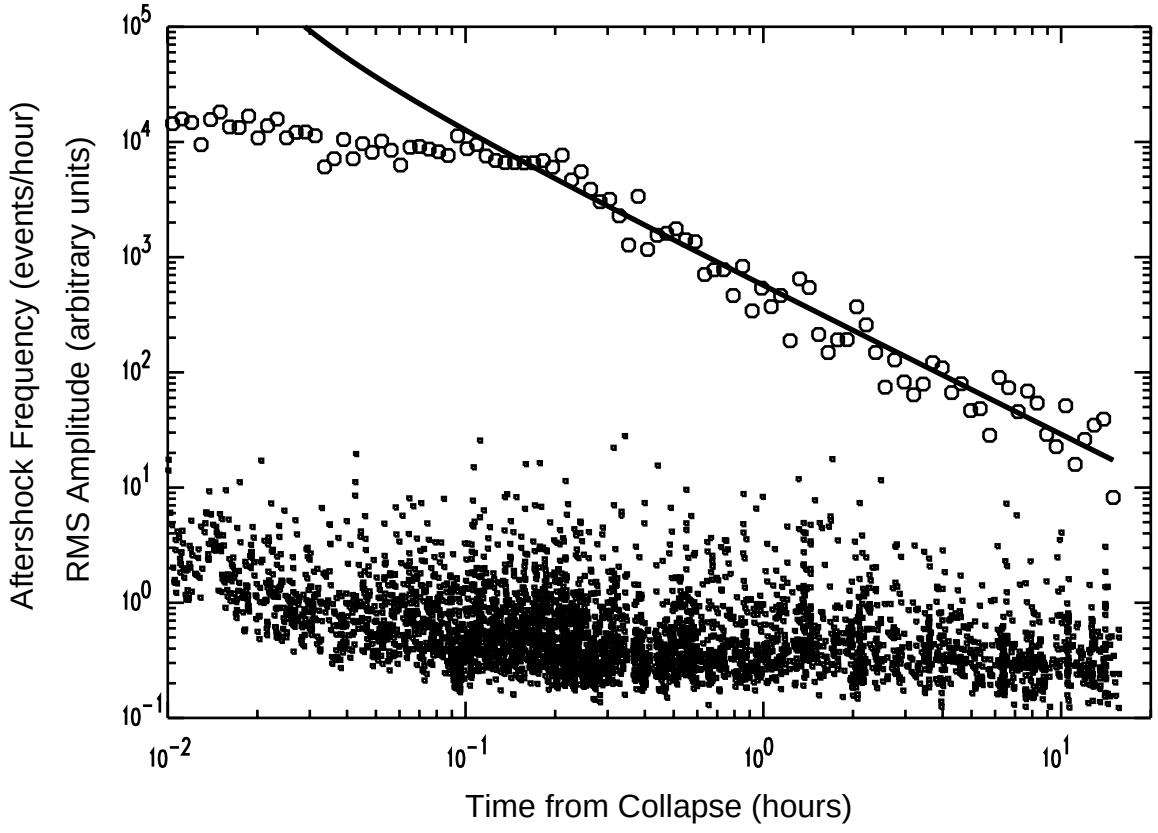

Figure 6: Event rate (circles) and the modified Omori law fit (line). The RMS amplitude of each aftershock is also plotted (small symbols) on an arbitrary scale to show the time range over which aftershock counting is complete.

We obtained a layer over a half-space model of seismic velocities. The layer contained glacial till, Freda sandstone and Nonsuch shale, thickness 320 m, Vp=3.80, Vs=1.60. The half-space contained the Copper Harbor conglomerate, Vp=5.46, Vs=3.07. Station corrections ranged from -18 ms to 20 ms for P waves and from -41 ms to 29 ms for S waves. This procedure resulted in event locations relative to the initial shot point.

For all aftershocks that were detected by a minimum of three stations, we determined P- and S-wave arrival times manually from a display of the vertical, radial and transverse components of motion. Radial and transverse components were obtained by rotating to the direction of ground zero. Arrival-time qualities were also assigned at this stage.

Arrival-time data quality decayed rapidly with distance from ground zero. For the innermost three stations (within 300 m of ground zero), the chance of obtaining a useable arrival time was 70% or so, depending on the specific station and phase. Data rates dropped to 30% at intermediate distance stations (300 m to 600 m) and to 10% or so at the outermost stations (over 1000 m). Percentages were calculated with respect to the number of three-station events as defined above. On average, such events yielded 4 P and 4 S arrivals, giving a total of 8 arrival times available for location.

We obtained microearthquake locations using an iterative, damped-least-squares (Geiger's) method. Arrival times were weighted by 1/T, where T was 4 ms for P waves and 12 ms for S waves. These values represent arrival time errors. Because initial results yielded a few large residuals, we added a reweighting scheme (Scales et al., 1988), which approximates the minimum L1 norm solution. The location calculation also included an estimate of the standard location error ellipsoid, using T, above, as estimates of the data error.

Aftershock Location Results

Plan and cross-section views of 135 aftershock locations are shown in Figure 8. These aftershocks were required to have 6 or more arrival times, magnitude of the major error-ellipsoid axis less than 50 m and RMS arrival time residual less than 7 ms.

The aftershock plan view shows a distribution that falls short of the unmined faces of the mine by over 50 m in places. Instead, the aftershocks concentrate along the boundary between explosively collapsed and unaltered pillars on the western, open edge of the collapsed panel. The cross-section views show an aftershock zone just under 100 m thick, bottoming at mine level. In the cross-section view to the north, the shallowest aftershocks fall closer to the open, western edge of the collapsed panel.

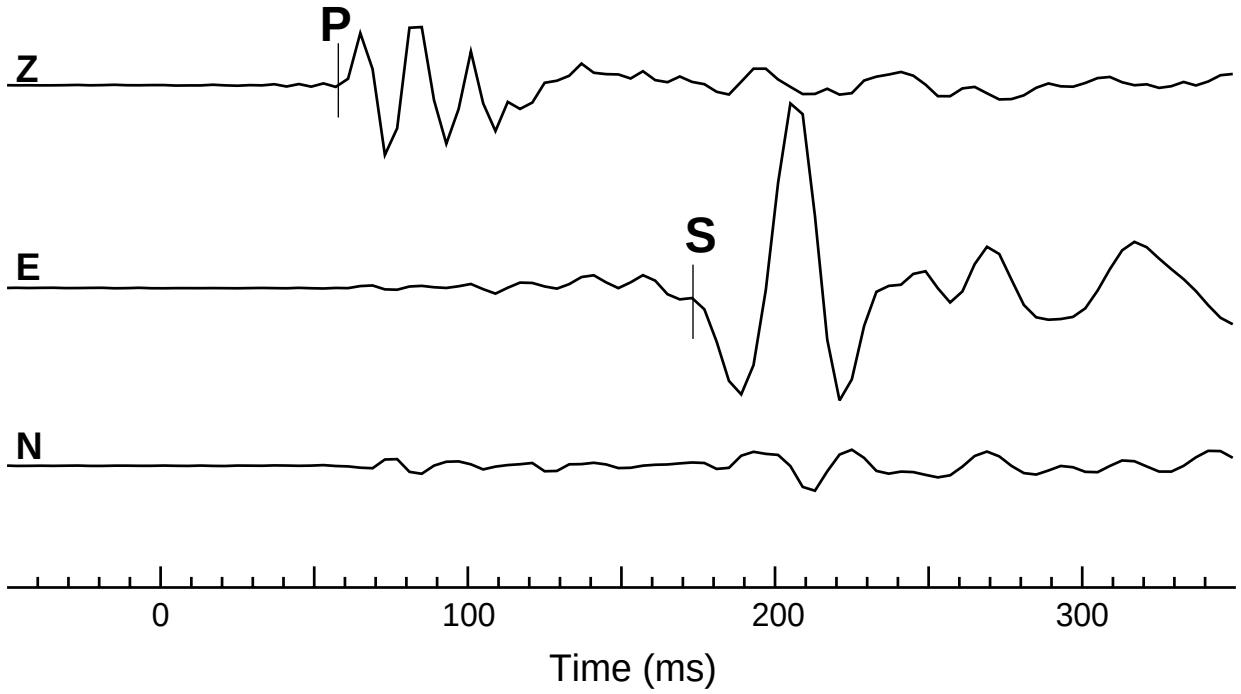

Figure 7: Vertical, east and north components of ground velocity for a typical shear-slip aftershock recorded at surface ground zero (station 13). Traces are plotted to a common scale.

The major axes of the location-error ellipsoids generally pointed in near-horizontal directions. The average major axis length was 25 m.

We observed some small-scale, space-time clustering of the aftershocks, but no gross changes in the distribution of activity with time.

Discussion

The aftershock distribution in map view is clearly asymmetric with respect to the collapsed panel, concentrating along the edge open to the mine. Few locations fall within 50 m of unmined faces of the panel. We should not be surprised to see the structural asymmetries of the mine reflected in the seismicity pattern. In fact, mine personnel claim convergence between the mine back and the floor is rarely seen within 100 m of the mine face during drift extension. Incomplete firing could also be a factor, but, in light of the convergence observations, may not be necessary to account for the asymmetrical aftershock pattern.

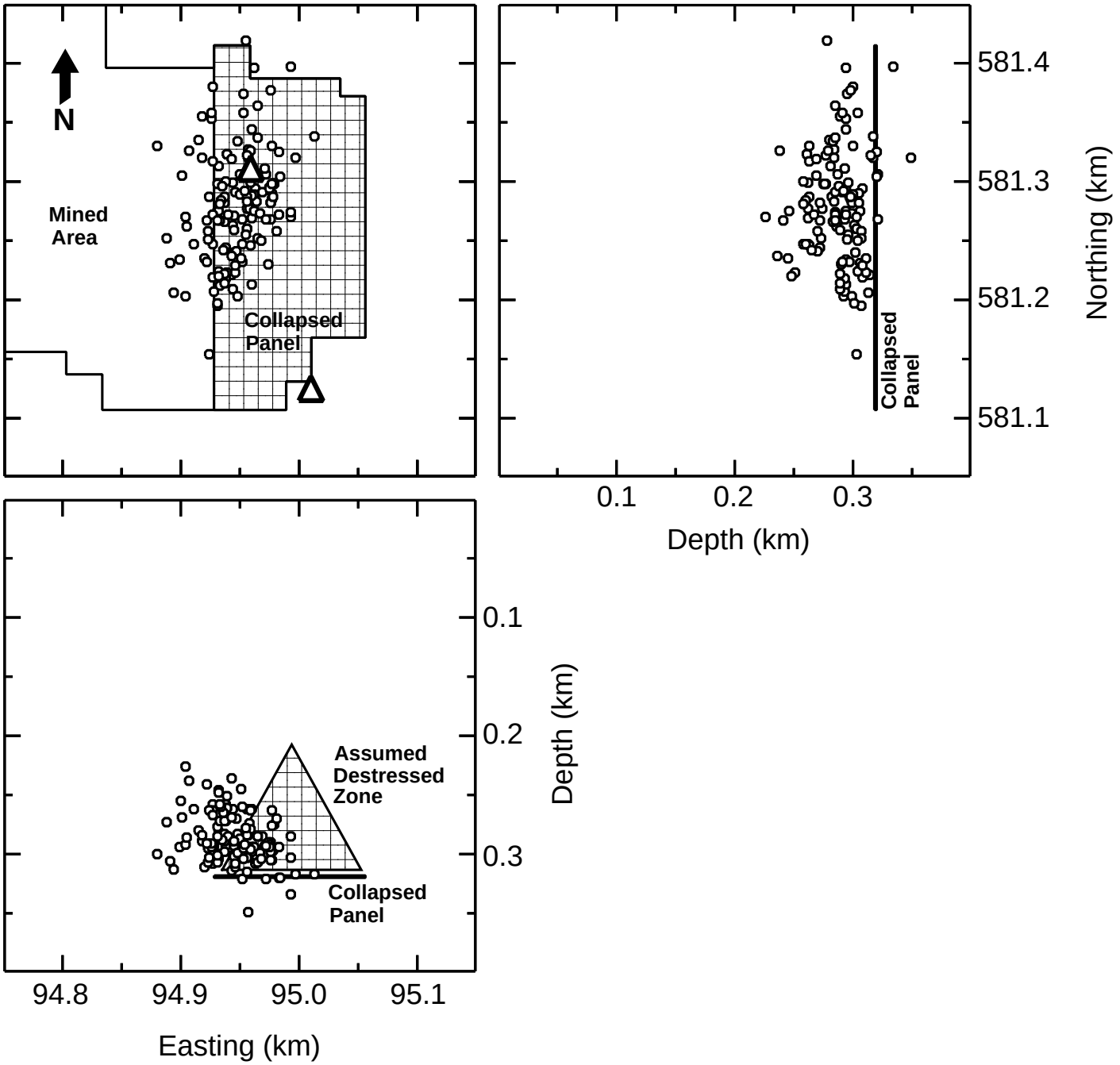

Figure 8: Map and cross-section views of aftershock locations. The mined area and the collapsed panel are indicated in map view. The collapsed panel is shown to scale in the cross-section views. The shaded triangle in the cross-section view looking north represents the assumed de-stressed zone used in modeling post-collapse stress redistribution.

In-situ measurements of stress changes in pillars adjacent to the collapsed panel were compared to predictions of psuedo-3D models by Golder Associates (Forsyth, 1995). These models assumed a "de-stressed" region directly above the collapse, defined as any material whose load was supported through the rubblized zone rather than through the adjacent pillars or unmined faces (Figure 8). The vertical dimension of the de-stressed zone was estimated to be 110 m by projecting a 60° angle from the edges to the middle of the short span (east-west) of the panel. This model produced post-collapse stresses on adjacent pillars that matched well with measurements, except for the pillars immediately adjacent to the collapsed panel (first row) where measured stresses were lower than model predictions.

If the aftershocks are thrusting or (sub-horizontally oriented) tensile crack events, they are consistent with a decrease in vertical stress following the collapse, and may indicate the extent of the de-stressed zone used in modeling. The vertical thickness of the aftershock zone was nearly the same as that of the assumed de-stressed zone. However, the aftershock zone in the cross-section view looking north indicates a thicker de-stressed zone along the open, western panel edge. If the de-stressed zone were modified to mimic the aftershock distribution, modeled stresses would be reduced along the western edge of the collapsed panel, enabling stress measurements in the first row of pillars to be matched more closely.

The shallowest aftershocks fell over 200 m below the surface, giving no evidence that deformation related to the collapse approached the near surface where the area's potable water aquifer lies. Of course, the lack of shallow seismicity does not prove that surface layers were unaffected by the collapse. Furthermore, we are not in a position to evaluate effects on the aquifer because we have little expertise in this area.

CONCLUSIONS

The explosively induced collapse of a panel in an underground room-and-pillar mine generated seismic signals that propagated to regional distances (as far as 1000 km). Magnitude (m_{bLg}) was estimated to be 3.1 at most from regional coda lengths.

The individual explosive charges emplaced in the pillars did not produce strong seismic signals, however, the failure of the pillars and the material above the working level did produce strong seismic signals. We estimated the mass and thickness of the displaced material to be 5.6×10^8 kg, and 11 m, respectively.

The largest aftershocks (moment magnitude 1.0) generated ground motions 2 orders of magnitude smaller than the collapse. The frequency of occurrence of the aftershocks decayed rapidly, following a modified Omori law with an exponent of 1.3. Of the located events, 90% occurred in the first 2 hours.

Aftershock locations defined a zone of stress redistribution and deformation following the collapse. The bottom of the zone fell at mine level, the top over 200 m below the surface, offering no evidence of deformation extending to the surface. Deformation was more extensive (shallower) near the western, open edge of the collapsed panel, consistent with the low stresses measured in the first row of pillars, relative to stresses predicted by post-collapse models.

In future work, we hope to obtain the focal mechanisms of aftershock events. This will give us better information about the stress changes above the collapsed panel and will help to understand the effects of the collapse on the surrounding mine structures. Because aftershocks were consistently recorded only at the innermost, three to five stations, traditional P-wave polarity methods will be inadequate and a full-waveform, moment-tensor type calculation will have to be performed. We anticipate that the stress field as well as fracture orientations can be inferred from the results.

ACKNOWLEDGMENTS

The success of our study was due, in great measure, to information provided by White Pine Mine personnel including reflection profiles and access to recording the shot break signal. Special thanks go to Daniel St. Don, Steve Brooks and Jochen Tilk. We also thank Diane Baker, Roy Boyd, Keith Kihara and Keith Dalrymple for help with data acquisition and Hans Hartse for retrieving seismic data from regional stations. This work is in

support of the DOE Comprehensive Test Ban Treaty Research and Development Program, ST482A, and was performed at Los Alamos National Laboratory under the auspices of the U.S. Department of Energy, Contract Number W-7405-ENG-36.

REFERENCES

Chaplin, M.P., Taylor S.R. and Toksoz, M.N. (1980). A coda-length magnitude scale for New England. *Earthquake Notes,* **51**,15-22.

Forsyth, W. (1995). Modeling results for Unit 43 test panel. Report to Copper Range Company, Golder Associates Ltd.

Geosphere, Inc. (1995). Seismic reflection survey for northeast mine expansion planning, White Pine Mine. Report to Copper Range Company.

Scales, J.A., Gersztenkorn, A. and Treitel, S. (1988). Fast Lp solution of large, sparse, linear systems: application to seismic traveltime tomography. *J. Comp. Phys*., **75**, 314-333.

Singh, S. and Herrmann, R.B. (1983). Regionalization of crustal coda Q in the continental United States. *J. Geophys. Res.,* **88**, 527-538.

Taylor, S.R. (1994). False alarms and mine seismicity, an example from the Gentry Mountain mining region, Utah. *Bull. Seism. Soc. Am.,* **84**, 350-358.

United Nations General Assembly (1996). Comprehensive Test Ban Treaty, **A/50/1027**, 26 August.

Utsu, T., Ogata, Y., Matsuura, R.S. (1995). The centenary of the Omori Formula for a decay law of aftershock activity. *J. Phys. Earth*, **43**, 1-33.